ACADEMIC PRESS

Available online at www.sciencedirect.com
SCIENCE DIRECT®

Journal of Catalysis 218 (2003) 288–295

JOURNAL OF CATALYSIS

www.elsevier.com/locate/jcat

Pd–Sn/Al_2O_3 catalysts from colloidal oxide synthesis II. Surface characterization and catalytic properties for buta-1,3-diene selective hydrogenation

S. Verdier,[a] B. Didillon,[b] S. Morin,[c] and D. Uzio [c,*]

[a] *Rhodia, CRA 52, rue de la Haie Coq, 93308 Aubervilliers Cedex, France*
[b] *Rhodia, CRL 85, rue des Frères Perret, 69192 St-Fons Cedex, France*
[c] *IFP, 1-4 avenue de Bois Préau, 92852 Rueil-Malmaison Cedex, France*

Received 9 October 2002; revised 23 January 2003; accepted 10 February 2003

Abstract

Surface and catalytic properties of alumina-supported bimetallic Pd–Sn catalysts prepared via a colloidal oxide synthesis have been studied. In-depth characterization of the supported metallic particles has been performed by techniques such as XPS, FTIR(CO), or LEIS, indicating a strong surface enrichment by Sn and suggesting a modification of the electronic properties of Pd ensembles. EXAFS results also demonstrate the core shell structure of the supported particles in agreement with our previous study of the oxidation state of tin species by ^{119}Sn Mössbauer spectroscopy. This in-depth characterization of the bimetallic catalysts allows us to demonstrate the influence of both Pd_xSn_y alloy formation and particle aggregation state on the selectivity of buta-1,3-diene hydrogenation.

Keywords: Bimetallic; Palladium; Tin; Colloidal oxide synthesis; Selective hydrogenation

1. Introduction

Extensive literature has demonstrated the beneficial effects which may be obtained by the promotion of a first metal with a second one. Increased stability toward sintering, improved resistance to poisons, and tuning of the selectivity toward the desired products have indeed been reported for a wide range of reactions such as selective hydrogenation of highly unsaturated compounds [1], hydrogenation of aromatics or N- and Cl-containing compounds [2,3]. The way the promoter modifies the catalytic behavior of the first metal can vary from bulk alloying or surface decoration to metal–oxide interactions because of the many possible structures occurring when preparing multicomponent catalysts [4,5]. Therefore, the control of the physicochemical properties of the particles is of major importance for obtaining the most homogeneous system in terms of particle size, composition, and structure to finally correlate them to the catalytic properties. In the case of the palladium–tin system, interesting catalytic properties have already been reported for this bimetallic catalysts particularly in selective hydrogenation reactions [6,7]. Nevertheless, the exact catalytic behavior of the different Pd–Sn phases (e.g., true Pd_xSn_y bulk alloy or metallic palladium interacting with oxidized tin Pd^0–Sn^x) has still to be investigated.

Colloidal oxide synthesis, a novel preparation method of metallic catalysts, has been developed in our laboratory. It consists in synthesizing colloidal particles of metallic oxides in aqueous solution and to deposit them onto the support. Subsequent low-temperature activation yields to the catalyst. This method has been successfully applied to the synthesis of monometallic palladium catalysts having a narrow size distribution centered on 1.8 nm [8].

In this work, different possibilities provided by colloidal oxide synthesis of preparing bimetallic catalysts have been applied to the preparation of alumina-supported Pd–Sn catalysts. In Part I of this study [9], we have demonstrated that these Pd–Sn catalysts are characterized by well-defined physicochemical properties such as their average particle size, their particle size distribution, and particle composition, especially when the catalyst is prepared by surface adsorption of tin(IV) onto colloidal PdO nanoparticles (here-

* Corresponding author.
E-mail address: denis.uzio@ifp.fr (D. Uzio).

0021-9517/03/$ – see front matter
doi:10.1016/S0021-9517(03)00064-2

after referenced as PdOSn route). In this case, it is indeed worth trying to correlate surface properties with catalytic ones.

Therefore, in this paper, the surface characterization of the metallic particles is first presented for PdOSn route, bimetallic Pd–Sn catalysts prepared by adsorption via the colloidal oxide synthesis. Then, catalytic performances in buta-1,3-diene selective hydrogenation are discussed, and, finally, a relation is established between the catalytic properties and the physicochemical properties of the active sites previously described.

Table 1
Main characteristics of the different catalysts

	PdO	PdSnA	PdOSn1	PdOSn2
Preparation method	PdO	Coimpregnation	PdO Sn	PdO Sn
Pd (wt%)	0.30	0.30	0.30	0.30
Sn (wt%)	–	0.33	0.17	0.17
Na (wt%)	0.70	0.05	0.70	0.70
Cl (wt%)	–	0.40	0.20	0.20
Particles	Isolated	Isolated	Isolated	Aggregated
Dispersion[a] (%)	63	21	45	3

[a] Dispersion, Pd_{surf}/Pd_{tot} determined by CO chemisorption measurements.

2. Experimental

2.1. Catalyst preparation

The preparation of the PdOSn catalyst has been fully described in detail in Part I of this work [9]. The first step of the preparation consists in synthesizing a basic PdO hydrosol (pH 12.1) by neutralization with soda of a palladium nitrate solution. To this PdO sol, a tin(IV) chloride solution is added to carry out the adsorption of tin(IV) species onto PdO nanoparticles. The resulting sol is then deposited by the wet impregnation technique onto alumina (γ-Al_2O_3 beads kindly supplied by Axens, $S_{BET} = 120\ m^2/g$). The catalyst is air-dried in a tubular reactor at 120 °C and further calcined at 200 °C for 2 h (ramp 5 °C/min). It is reduced under pure hydrogen at the desired temperature for 2 h (ramp 5 °C/min) before its characterization and catalytic evaluation. As determined by TEM in [9], PdOSn1 catalyst differs from PdOSn2 mainly by the aggregated character of its bimetallic particles resulting from a longer preparation time. This aggregated state leads to a low dispersion of the metallic phase as measured by the dynamic CO chemisorption method.

For comparison, two other catalysts were prepared. The first one is a monometallic palladium catalyst referenced as PdO and prepared via the colloidal oxide route by the same way as PdOSn except that the tin solution was not added. The second one is a bimetallic Pd–Sn catalyst referred to as PdSnA prepared by conventional coimpregnation of an acidic solution of both palladium nitrate and tin(IV) chloride.

The characteristics of the different catalysts are listed in Table 1.

2.2. Characterization

XPS (X-ray photoelectron spectroscopy) measurements were performed on a Kratos Axis Ultra spectrometer using a monochromatic Al-K_α radiation ($E_0 = 1486.6$ eV). Samples were reduced in the laboratory under H_2 at 200 °C for 2 h (ramp 5 °C/min) and subsequently sealed under secondary vacuum to be further introduced in the analysis room of the spectrometer without being exposed to air. Experiments were made under secondary vacuum ($<10^{-9}$ mbar) and resolution was about 0.5 eV. Spectra are calibrated with the O of alumina 1s core level at 530.8 eV and photopeak deconvolution is obtained using Gaussian-type curves.

LEIS (low energy ion spectroscopy) measurements were performed at the University of Eindhoven with a Calipso Instrument by Prof. H.H. Brongersma's team. Pd–Sn catalysts were studied after in situ reduction under 200 mbar hydrogen at 200 °C for 2 h in the treatment room of the spectrometer (controlled atmosphere and temperature). Despite their close atomic numbers ($Z_{Pd} = 46$, $Z_{Sn} = 50$), distinction between Pd and Sn could be achieved using 5 keV Ne^+ ions. The scattering angle was set at 145°. The first monolayer was investigated under an ionic current of about 1.5–2 nA over an estimated analyzed surface area of 1 mm^2. Submonolayers were analyzed after a stronger ionic current treatment. Pd and Sn were quantified using as references the signals recorded after ionic erosion for foils of each metal.

EXAFS (extented X-ray absorption fine structure) experiments were carried out on Station 4 of the LURE facility (Laboratoire pour l'Utilisation du Rayonnement Electromagnétique, Orsay, France) using the synchrotron radiation from the DCI storage ring running at 1.85 GeV with an average current of 250 mA. Both the Pd and Sn K edges (respectively, at 24,350 and 29,190 eV) were monitored in the transmission mode using a double Si(111) crystal monochromator and two ion chambers as detectors. Signal to noise ratio was optimized by acquiring multiple scans for every spectrum. Activation of the catalysts was similar to that reported for XPS measurements. Reduced catalysts were further introduced under Ar in the transmission cell of the spectrometer without being exposed to air. Data analysis employed a standard package [10]. Amplitude and phase functions for fitting Pd–O (respectively Sn–O) and Pd–Pd (respectively Sn–Sn) shells were obtained from PdO (respectively SnO and SnO_2) powder standards and Pd (respectively Sn) foil.

FTIR spectra of probe CO molecules were obtained on a Fourier Nexus spectrometer from Nicolet. Catalyst samples (about 10 mg/cm^2) were pressed under about 200 kg/m^2 into self-supporting disks (16 mm in diameter) and loaded in the in situ IR cell. The catalyst first undergoes a thermal cleaning treatment at 200 °C for 16 h under secondary vacuum (about 10^{-6} mbar). It is then reduced under 400 mbar H_2 at 200 °C for 2 h. After cooling to 30 °C under secondary

vacuum, a 20 mbar CO pulse (1.38 µmol CO) is introduced in the IR cell and a spectrum (200 interferograms accumulated) is collected in transmission mode with a resolution of 0.5 cm^{-1}. CO desorption is then monitored under vacuum after evacuation of the cell. All results reported herein are difference spectra, corresponding to the IR spectra of the samples plus adsorbed CO minus the IR spectra of the clean samples. CO coverage (θ) is considered to be equal to 1 after the CO pulse (saturated sample). The linear to bridge ratio (L/B) is measured at $\theta = 1$ considering that the molar extinction coefficients do not depend on the adsorption mode.

2.3. Catalytic measurements

Buta-1,3-diene selective hydrogenation tests were performed in liquid phase using a laboratory scale stainless-steel batch reactor working under static conditions with variation of the concentration of reactants and products over time. Two grams of catalyst reduced for 2 h under H_2 at the desired temperature (ramp 5 °C/min) are put in contact with buta-1,3-diene diluted in *n*-heptane at 17 °C under 10 bar of H_2 and high stirring velocity. Experimental conditions were previously selected in order to avoid mass transfer limitations. The reacting mixture is sampled over time and analyzed by gas chromatography.

The modeling of the reactants concentrations as a function of time is performed using a kinetic model proposed by Boitiaux et al. [11] in which a Langmuir–Hinshelwood formalism is used to describe a Horiuti–Polanyi mechanism [12]. In this model, no distinction is made between *cis*- and *trans*-but-2-ene and it is assumed that but-1-ene and but-2-enes have the same adsorption constants K. Moreover, retro-isomerization of but-2-ene (thermodynamically stable isomer) to but-1-ene is neglected. Finally, the adsorption constant of butane is considered to be negligible compared to that of unsaturated hydrocarbons. Kinetic constants k_i and the adsorption constants ratio $K_{BD}/K_{Butenes}$ (BD = buta-1,3-diene) are determined using a time differential system resolved by a Gear-type integrator. Minimization of parameters is realised by the Levenberg–Marquardt method with a confidence interval of ±5%. The kinetic constants k_i are expressed as turn-over numbers (TON, $mol/(s\,mol_{surface\ Pd})$) using the palladium dispersions measured by CO chemisorption (see Table 1).

3. Results

3.1. Catalyst characterization

PdOSn2, prepared via the surface adsorption route, has been extensively characterized regarding its surface properties.

XPS spectra of this catalyst after calcination and reduction at 200 °C were measured in order to determine the electronic state of both metallic components. Table 2 presents the binding energies of the principal Sn and Pd $3d_{5/2}$ X-ray photoemission transitions shown in Fig. 1.

Table 2
Binding energies of the Sn $3d_{5/2}$ and Pd $3d_{5/2}$ transitions for the PdOSn2 catalyst after calcination and reduction at 200 °C

$3d_{5/2}$ (eV)	Pd	Sn
After calcination at 200 °C	337.5	486.4
After H_2 reduction at 200 °C	336.5 (21%)	486.3 (68%)
	335.0 (79%)	484.9 (32%)

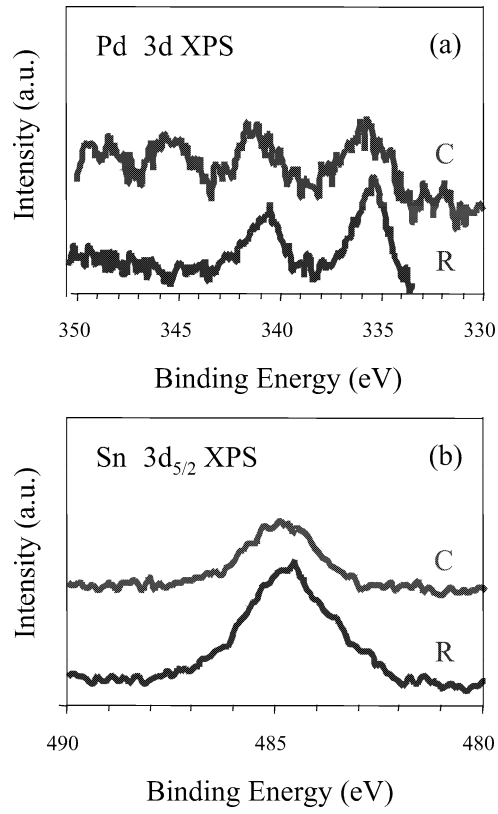

Fig. 1. (a) Pd 3d and (b) Sn $3d_{5/2}$ photoemission core-level spectra from PdOSn2 after calcination (C) and reduction (R) at 200 °C.

After calcination, photopeaks are characteristic of oxidized species for both tin and palladium. After reduction at 200 °C, about 32% of metallic tin Sn^0 is detected at 484.9 eV. Concerning Pd, a major component at 335.0 eV corresponding to Pd^0 is observed together with a weaker binding energy (BE) state at 336.5 eV that can be ascribed to a more "oxidized" palladium species.

LEIS spectra obtained for the PdOSn2 catalyst after in situ reduction at 200 °C are presented in Fig. 2. These spectra are characterized by 2 retrodiffusion peaks at about 2378 and 2555 eV, respectively corresponding to retrodiffusion by Pd and Sn atoms.

Surface concentrations deduced from LEIS spectra analysis are reported in Table 3 as a function of the investigated monolayers. As erosion increases, the concentration of palladium increases whereas that of tin decreases, indicating a

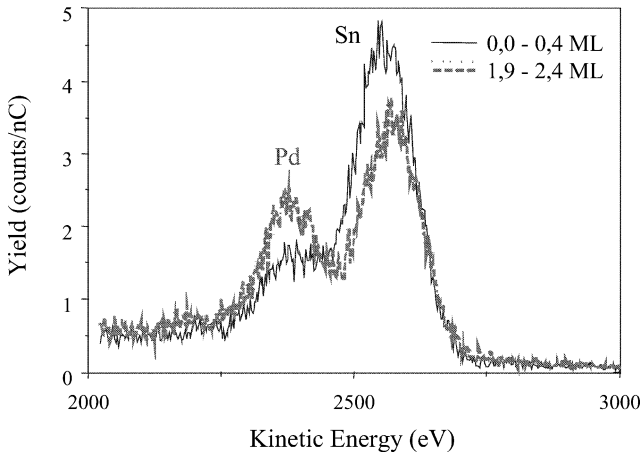

Fig. 2. Erosion profile under a 5 keV Ne^+ ion beam of the PdOSn2 catalyst after in situ reduction at 200 °C. ML, monolayer.

Table 3
Surface composition of the first atomic monolayers of the PdOSn2 catalyst after in situ reduction at 200 °C

at%	Pd	Sn
0.0–0.4 ML	18	82
1.9–2.4 ML	38	62

Table 4
Nature and number of the neighbors at the Pd and Sn K edge for PdOSn2 catalysts after calcination and reduction at 200 °C

	Nature	N (±0.5)	d (Å)	$\Delta\sigma$ (Å^2)
Pd K edge				
After calcination				
First neighbor	O	5.0	1.98	0.03
Second neighbor	Pd	3.0	3.05	0.05
	Pd	4.3	3.31	0.07
After reduction				
First neighbor	Pd	8.2	2.74	0.04
Sn K edge				
After calcination				
First neighbor	O	5.5	1.99	0.03
After reduction				
First neighbor	O	3.0	2.08	0.04
Second neighbor	Pd	3.4	2.70	0.05

pronounced surface enrichment by tin with respect to palladium.

EXAFS results after calcination and reduction steps are summarized in Table 4. The structural transformations upon reduction can be observed on the Pd and Sn K-edge radial distribution functions (RDFs) (see Fig. 3).

At the Sn K edge, Sn stands after calcination in an environment similar to that of cassiterite SnO_2 (coordination number = 6; $d_{Sn–O} \approx 2.1$ Å). After reduction, Sn still remains mainly surrounded by O but second neighbors are detected at an interactomic scattering distance of about 2.70 Å. Such a value differs from the Sn–Sn nearest neighbor distance varying from 2.80 to 3.02 Å in bulk β- and α-Sn structures [13]. Supposing that hypothetical Pd–Sn ensembles adopt a cfc-like structure, the Pd–Sn distance should be close to 2.74 Å as in metallic palladium and possibly smaller because of Sn charge polarization due to the difference of Pauling electronegativities (χ[Sn] = 1.96 and χ[Pd] = 2.20). Therefore, this shell can reasonably be attributed to Pd atoms. Note that this attribution is coherent with the presence of tin alloyed with palladium as detected by ^{119}Sn Mössbauer spectroscopy [9].

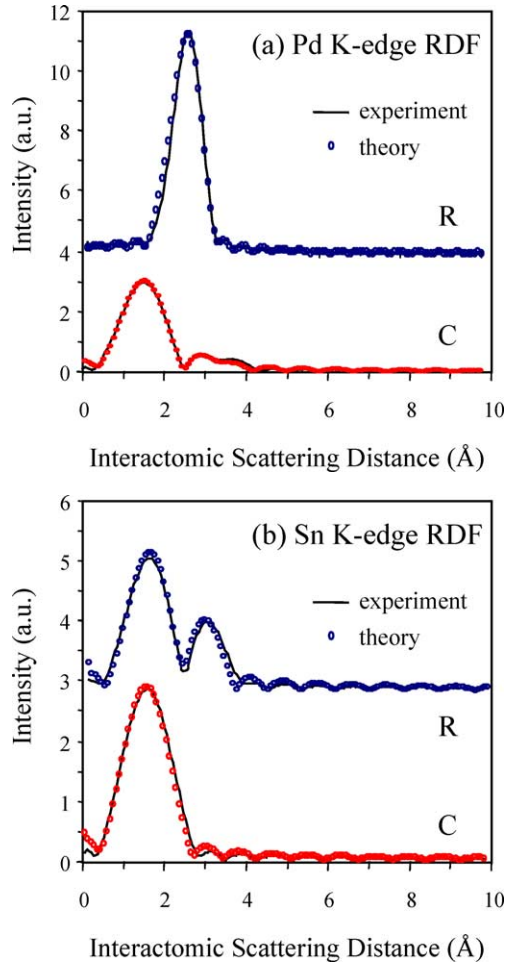

Fig. 3. (a) Pd and (b) Sn K-edge pseudoradial distribution functions obtained from PdOSn2 catalysts after calcination (C) and reduction (R) at 200 °C.

At the Pd K edge, the environment of palladium after calcination is typical of PdO with O as first neighbors and Pd as second ones. After reduction, only metallic neighbors are identified at an interatomic scattering distance of 2.74 Å typical of metallic palladium. The coordination number is also in agreement with the size (2 nm) of the elementary particles forming the aggregates observed by TEM [9]. Thus, no tin scatterers could be detected for PdOSn2. Actually, the Pd K-edge fitting parameters for this catalyst are similar to those of PdO. We will discuss more precisely the absence of tin later.

The FTIR(CO) study was made on the PdOSn2 catalyst and on the mono- and bimetallic reference catalysts, PdO

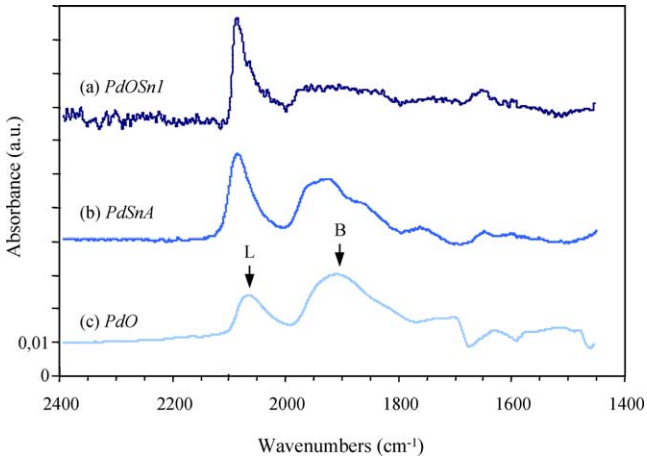

Fig. 4. FTIR spectra of CO adsorbed on (a) PdOSn2, (b) PdSnA, and (c) PdO after thermal treatment and reduction at 200 °C.

Table 5
L/B ratio at CO coverage $\theta = 1$ for the different catalysts after reduction at 200 °C

	PdO	PdSnA	PdOSn2
L/B	0.3 ± 0.1	0.6 ± 0.1	1.5 ± 0.5

and PdSnA. After CO adsorption, the spectra display two main bands (see Fig. 4).

The band at 2000–2100 cm^{-1} is ascribed to CO linearly (L) adsorbed onto Pd while the broader one between 1800 and 2000 cm^{-1} is typical of "bridged" (B) CO coordinated to 2 or 3 palladium atoms [14]. The bands between 1700 and 1500 cm^{-1} are relative to hydrogenocarbonate species resulting from adsorption of CO_2 formed by the Boudouart reaction ($2CO \rightarrow C + CO_2$) over palladium. The absence of any detectable bands at 2100–2150 cm^{-1} typical of adsorption of CO on oxidized $Pd^{\delta+}$ species confirms that palladium is totally reduced which is consistent with Pd K-edge EXAFS results.

The values of the linear to bridged ratio L/B determined at CO coverage $\theta = 1$ are reported in Table 5. The L/B ratio is higher for the two bimetallic catalysts which is related to the dilution of surface Pd atoms by Sn avoiding the formation of bridged species. In the case of PdOSn2, this ratio is strongly enhanced in agreement with the Sn surface enrichment demonstrated by LEIS.

The vibration frequency of linearly adsorbed CO was extrapolated at null CO coverage in Fig. 5 after a saturation pulse and desorption at room temperature. The results are reported in Table 6.

At $\theta = 0$, i.e., without any dipole–dipole interaction, the linear vibration frequency is shifted toward higher wavenumbers for the bimetallic catalysts with respect to the monometallic one. In the case of PdOSn1, this blue shift measured by $\Delta(\theta = 0) = \bar{\nu}_{CO}^{linear}$ (PdOSn1) $- \bar{\nu}_{CO}^{linear}$ (PdO) is particularly pronounced: more than 30 cm^{-1}. It indicates a significant decrease of the Pd–CO bond strength related to

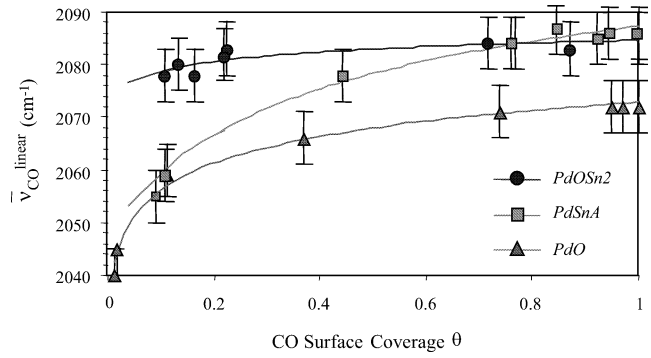

Fig. 5. Variation of $\bar{\nu}_{CO}^{linear}$ with θ for PdOSn2, PdSnA, and PdO reduced at 200 °C after desorption at room temperature of CO adsorbed at saturation.

Table 6
Vibration frequency of linearly adsorbed CO $\bar{\nu}_{CO}^{linear}$ at $\theta = 0$ and $\theta = 1$ for the different catalysts after reduction at 200 °C

	PdO	PdSnA	PdOSn2
$\bar{\nu}_{CO}^{linear}(\theta = 1)$	2065 ± 5	2086 ± 5	2085 ± 5
$\bar{\nu}_{CO}^{linear}(\theta = 0)$	2040 ± 5	2050 ± 5	2075 ± 5

a lower extent of retrodonation phenomenon from Pd to CO as defined in the Blyholder model [15].

3.2. Catalytic properties

Buta-1,3-diene hydrogenation is a widely used model reaction to investigate surface modification by promoters or alloy formation [16]. The reaction is usually described using the network presented in Fig. 6 [11,17]. Direct hydrogenation of buta-1,3-diene to butane is not considered here because it is assumed not to occur over palladium-based catalysts [18].

An example of the kinetic modeling described in the experimental section is presented in Fig. 7 in the case of the monometallic PdO catalyst.

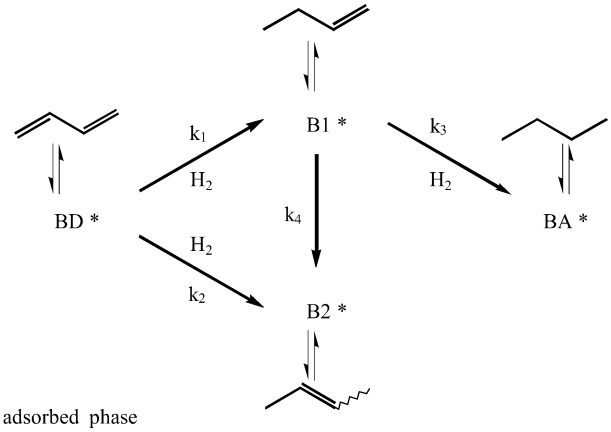

Fig. 6. Reaction network for the selective hydrogenation of buta-1,3-diene. BD, buta-1,3-diene; B1, but-1-ene; B2, but-2-ene; and BA, butane.

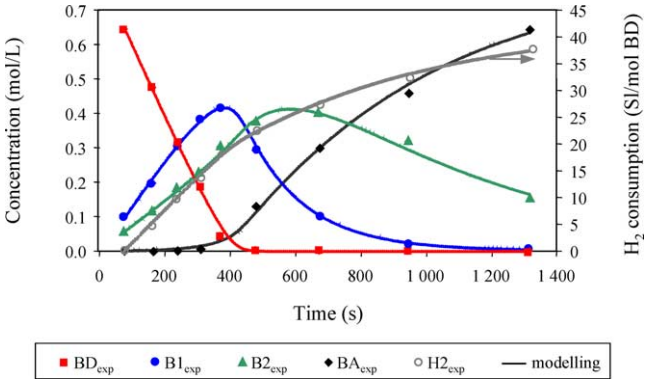

Fig. 7. Experimental (symbols) and kinetic modeling (lines) of buta-1,3-diene selective hydrogenation over the PdO catalyst.

Using the modeled kinetic and adsorption constants, the kinetic selectivity r is defined as

$$r = \frac{k_1 K_{BD}}{(k_3 + k_4) K_{B1}} \qquad \text{BD} \xrightarrow{k_1} \text{B1} \begin{cases} \xrightarrow{k_3} \text{BA} \\ \xrightarrow{k_4} \text{B2} \end{cases}.$$

This parameter is representative of the selectivity for the consecutive hydrogenation of buta-1,3-diene to but-1-ene. When $r > 1$, the formation of but-1-ene is more important than its consumption.

Considering Table 7, addition of tin impacts in a different manner the kinetic selectivity r. When compared to the monometallic PdO catalyst, r slightly decreases for the coimpregnated PdSnA catalyst whereas it sharply increases for the PdOSn2 catalyst prepared via the colloidal oxide synthesis. As kinetic constants, expressed in turn-over numbers (TON), do not show significant discrepancies between the different catalysts, the main contribution of the variation of the kinetic selectivity is ascribed to the adsorption constants ratio $K_{BD}/K_{Butenes}$. In the case of the PdOSn2 catalyst, formation of but-1-ene is favored compared to its consumption because the $K_{BD}/K_{Butenes}$ ratio increases, indicating that olefin adsorption is much more destabilized than diene adsorption. Thus, the olefin would easily desorb before hydrogenation to butane.

Despite the close similarities in their preparation methods, PdOSn1 and PdOSn2 exhibit different physicochemical properties as described in [9]. Briefly, the supported metallic particles of PdOSn2 are aggregated whereas those of PdOSn1 are isolated. It implies a different behavior toward Pd_xSn_y formation upon reduction. Indeed, whereas alloy formation is observed after reduction at 200 °C for PdOSn2, the allied phase is identified by ^{119}Sn Mössbauer spectroscopy only by 300 °C for PdOSn1. As can be seen in Table 8, PdOSn1 and PdOSn2 also exhibit a different behavior in catalysis.

Table 7
Turn-over frequencies (TON) (mol/(s $mol_{surface\ Pd}$)) and kinetic selectivity r for the different catalysts after reduction at 200 °C

	PdO	PdSnA	PdOSn2
TON_1 (BD → B1)	5.8	8.2	11.6
TON_2 (BD → B2)	3.6	2.4	6.6
TON_3 (B1 → BA)	2.6	7.3	2.3
TON_4 (B1 → B2)	4.7	8.9	2.5
$K_{BD}/K_{Butenes}$	22.0	11.2	80.9
r	17.3	5.7	194.4

$T_{red} = 200$ °C.

Table 8
Comparison between PdOSn1 and PdOSn2 catalytic properties and alloy formation

	PdOSn1			PdOSn2
T_{red} (°C)	200	300	400	200
TON_1 (BD → B1)	6.5	5.2	6.5	11.6
TON_2 (BD → B2)	3.2	4.0	3.6	6.6
TON_3 (B1 → BA)	5.9	2.4	1.2	2.3
TON_4 (B1 → B2)	8.6	2.0	1.5	2.5
$K_{BD}/K_{Butenes}$	9.1	15.2	11.1	80.9
R	4.1	18.3	27.1	194.4
Alloyed Sn (at%)	0	10 (PdSn)	49 (Pd_2Sn)	40 (Pd_2Sn)

For the same reduction temperature, $T_{red} = 200$ °C, PdOSn2 is more selective than PdOSn1 by 2 orders of magnitude. The loss of selectivity in PdOSn1 cannot be related to the amount of Pd_xSn_y alloy. Indeed, for about the same proportion of Pd_2Sn alloy, obtained after reduction at 400 °C for PdOSn1, the kinetic selectivity slightly increases but the difference remains still significant (1 order of magnitude), indicating that aggregation state of the supported particles plays a major role in controlling the kinetic selectivity of the catalyst. The aggregation state does not modify the TON_i values which are in the same range for both PdOSn1 and PdOSn2. However, it implies a significant increase of the adsorption constants ratio $K_{BD}/K_{Butenes}$.

Considering PdOSn1, the kinetic selectivity increases with the reduction temperature. In this case, the $K_{BD}/K_{Butenes}$ ratio remains almost constant but the kinetic constants relative to the hydrogenation and double bond isomerization of but-1-ene (TON_3 and TON_4) strongly decrease as shown on Fig. 8. When the reduction temperature increases, the aggregation state of PdOSn1 does not vary; the supported

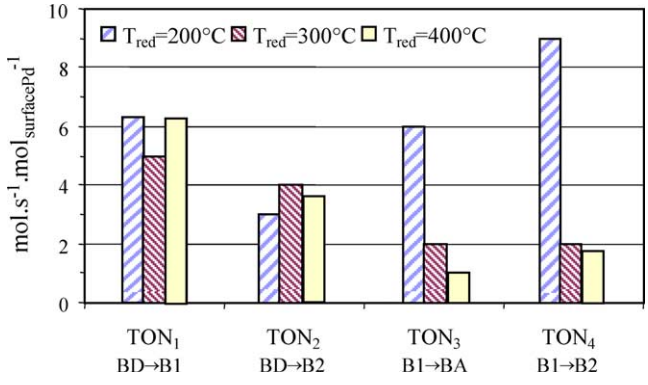

Fig. 8. Influence of the reduction temperature on the kinetic constants TON_i of the PdOSn1 catalyst.

metallic particles remain indeed isolated. Thus, the modification of the chemical steps relative to but-1-ene can be associated with the increasing proportion of alloy in the catalyst.

4. Discussion

As far as the oxidation state of tin in PdOSn1 is concerned, the XPS spectra indicating the presence of metallic tin after reduction are consistent with the identification of the allied phase Pd_2Sn in ^{119}Sn Mössbauer spectroscopy experiments (see [9]). The XPS quantification (about 32% of Sn^0) is in rather good agreement with the value determined by the latter technique (about 40% of Sn^0).

Moreover, the characterization of the alloyed phase allows us to be precise about the nature of the metallic neighbors at the Sn K edge in the EXAFS study. The attribution of this metallic shell to Pd atoms was already reported for Pd–Sn catalysts prepared by controlled surface organometallic reaction (CSOR) [6,19]. These works also reported the absence of tin neighbors at the Pd K edge. To explain this result, we assume that both the Pd/Sn ratio of 2 and the proportion of alloyed tin do not allow the characterization of tin scatterers.

Concerning the localization of both elements in the metallic particles of PdOSn2, LEIS results indicate a strong surface enrichment of tin as expected from thermodynamic considerations [20]. Indeed, tin has the lowest sublimation energy ($\Delta H_{sub}(Sn) = 296$ kJ/mol $< \Delta H_{sub}(Pd) = 357$ kJ/mol [21]) and the lowest surface free energy ($\gamma(Sn) = 0.7$ J/m^2 $< \gamma(Pd) = 2.1$ J/m^2 [19]) with respect to palladium. Such an enrichment is confirmed by the dilution of surface palladium ensembles by tin as demonstrated by the increase of the L/B ratio in FTIR(CO). Note that the presence of tin in the outer shells of the metallic particles is consistent with the preparation method consisting in adsorbing tin(IV) molecular species onto PdO colloidal nanoparticles.

The pronounced blue shift ($\Delta > +30$ cm^{-1}) observed in FTIR(CO) indicates a modification of the electronic properties of palladium. On the one hand, such a value is quite high compared to the ones usually reported for bimetallic catalysts: $|\Delta| < 10$ cm^{-1} [21]. This shift is significant of the decrease of the metal–carbon bond strength and could be interpreted by an electronic donor effect of Sn to Pd in agreement with Pauling electronegativity ($\chi[Sn] = 1.96$ and $\chi[Pd] = 2.20$) as already observed in the case of PtSn-supported catalysts [22]. It has been checked that Cl or Na, also present on the catalysts, may not create such an effect. No vibration at 2150 cm^{-1}, ascribed as CO adsorbed on Pd oxide PdO [14], is observed in agreement with EXAFS data which excluded the presence of O in the neighborhood of Pd. Higher reduction temperature promotes Pd–Sn alloy formation and mainly modifies the kinetic constants of but-1-ene consumption (B1 → BA and B1 → B2). Dilution of Pd by Sn at the surface of particles may inhibit surface mobility of adsorbed species (hydrocarbons and hydrogen).

The increase of $K_{Bd}/K_{Butenes}$ for aggregated particles shows that adsorption of olefins is strongly disfavored when compared to diolefin adsorption. This modification may be related to a variation of electronic properties when metallic particles are in contact as shown by Pagès [23] who observed that binding energy of Pd/Al_2O_3 decreases from 334.7 to 334.4 eV for aggregated particles and isolated ones. The adsorption strength of unsaturated compounds is indeed very dependent on the electronic density of the surface atoms.

In this light, alloy formation and aggregated state influence the reaction pathway at two different steps of the catalytic pathway: at the adsorption/desorption step of compounds for aggregated state and at the chemical reaction step in adsorbed state for alloy formation.

5. Conclusion

Alumina-supported bimetallic Pd–Sn catalysts prepared by the colloidal oxide synthesis have been studied in order to correlate catalytic performances and physicochemical properties of particles. It has been demonstrated that Pd_xSn_y species strongly modify the selectivity for buta-1,3-diene hydrogenation. The alloy content controls the intrinsic kinetic constants of the catalyst whereas the aggregated state of the bimetallic particles is proposed to play an important role on the adsorption step of reactants.

Acknowledgments

The authors gratefully acknowledge the IFP Physics & Analysis Department for technical support by carrying out the different characterization experiments and for help in interpreting the results. V. Coupard from IFP Lyon is also acknowledged for fruitful discussions on the kinetic model.

References

[1] J.P. Boitiaux, J. Cosyns, M. Derrien, G. Leger, Hydrocarbon Process. 64 (1985) 51.
[2] A.J. Renouprez, A. Malhomme, J. Massardier, M. Cattenot, G. Bergeret, Stud. Surf. Sci. Catal. 130c (2000) 2579.
[3] R. Ohnishi, W.L. Wang, M. Ichikawa, Appl. Catal. A 113 (1994) 29.
[4] V. Ponec, G.C. Bond, Catalysis by Metals and Alloys, Elsevier, Amsterdam, 1995.
[5] J.J. Burton, E. Hyman, D.G. Fedak, J. Catal. 37 (1975) 106.
[6] S.H. Choi, J.S. Lee, J. Catal. 193 (2000) 176.
[7] H.R. Aduriz, P. Bodnariuk, B. Coq, F. Figueras, J. Catal. 129 (1991) 47.
[8] B. Didillon, E. Merlen, T. Pagès, D. Uzio, Stud. Surf. Sci. Catal. 118 (1998) 41.
[9] See Part I.
[10] (a) B.K. Teo, EXAFS: Basic Principles and Data Analysis, Springer, Berlin, 1986;
(b) A. Michalowicz, PhD thesis, University Paris Val de Marne, 1990.
[11] J.P. Boitiaux, J. Cosyns, N. Derrien, G. Léger, AIChE National Meeting, Houston, March 24, 1984.

[12] J. Horiuti, M. Polanyi, J. Chem. Soc., Faraday Trans. 30 (1934) 1164.
[13] A.F. Wells, in: Structural Inorganic Chemistry, Clarendon Press, Oxford, 1975, p. 121.
[14] C. Binet, A. Jadi, J.C. Lavalley, J. Chim. Phys. 86 (1989) 451.
[15] G.J. Blyholder, J. Phys. Chem. 68 (1964) 2772.
[16] V. Ponec, G.C. Bond, in: Catalysis by Metals and Alloys, Elsevier, Amsterdam, 1995, p. 500.
[17] J. Goetz, D.Y. Murzin, M. Ulischenko, R. Touroude, Chem. Eng. Sci. 51 (1996) 2879.
[18] J.P. Boitiaux, J. Cosyns, E. Robert, Appl. Catal. 35 (1987) 193.
[19] A.F. Lee, C.J. Baddeley, C. Hardacre, G.D. Moggridge, R.M. Ormerod, R.M. Lambert, J.P. Candy, J.M. Basset, J. Phys. Chem. B 101 (1997) 2797.
[20] V. Ponec, G.C. Bond, Stud. Surf. Sci. Catal. 95 (1995) 175.
[21] R.C. Weast, CRC Handbook of Chemistry and Physics, 69th ed., The Chemical Rubber Company, Cleveland, 1988.
[22] J. Burch, J. Catal. 71 (1981) 348 and 360.
[23] T. Pagès, PhD thesis, University Paris VI, 1998.